

# Interplay between Glass Formation and Liquid–Liquid Phase Separation Revealed by the Scattering Invariant

Stefano Da Vela, Nafisa Begam, Danylo Dyachok, Richard Santiago Schäufler, Olga Matsarskaia, Michal K. Braun, Anita Girelli, Anastasia Ragulskaya, Alessandro Mariani, Fajun Zhang,\* and Frank Schreiber



Cite This: *J. Phys. Chem. Lett.* 2020, 11, 7273–7278



Read Online

ACCESS |



Metrics & More

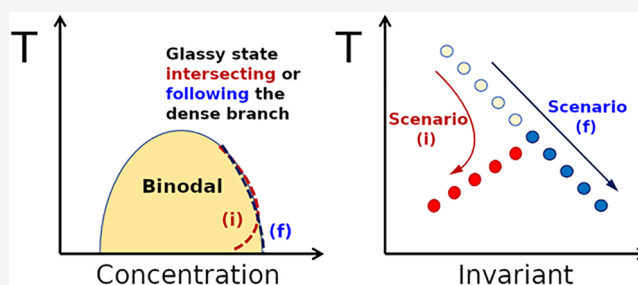


Article Recommendations



Supporting Information

**ABSTRACT:** The interplay of the glass transition with liquid–liquid phase separation (LLPS) is a subject of intense debate. We use the scattering invariant  $Q$  to probe how approaching the glass transition affects the shape of LLPS boundaries in the temperature/volume fraction plane. Two protein systems featuring kinetic arrest with a lower and an upper critical solution temperature phase behavior, respectively, are studied varying the quench depth. Using  $Q$  we noninvasively identify system-dependent differences for the effect of glass formation on the LLPS boundary. The glassy dense phase appears to enter the coexistence region for the albumin– $\text{YCl}_3$  system, whereas it follows the equilibrium binodal for the  $\gamma$ -globulin–PEG system.



The phenomenon of arrested phase separation in colloid and protein solutions has been intensively studied experimentally,<sup>1–9</sup> theoretically,<sup>10</sup> and in simulations<sup>11,12</sup> because it provides fundamental insights into the nature of gels and glasses. If a glassy state is approached by the dense branch of a liquid–liquid demixing gap, the liquid–liquid phase separation (LLPS) comes to a halt, and a dynamically arrested state is formed. If the amount of the denser phase is sufficient, this state spans the entire sample. The resulting structures are relevant for a broad range of applications from food industry to material science to biology.<sup>13–15</sup> A still largely unsolved question is the effect of the glass transition on the apparent shape of the binodal in such systems.<sup>2,3,16–22</sup> Under conditions of arrested phase separation, the concentration of the dense phase may decrease with the quench depth because of the dynamic arrest occurring at concentrations lower than the ones expected based on the equilibrium binodal (scenario i, “intersecting”, in Figure 1). Alternatively, it may follow the dense branch of the binodal (scenario f, “following”, in Figure 1).

Scenario i is supported by studies employing lysozyme solutions as a model system. For shallow temperature quenches,<sup>4</sup> LLPS proceeds to completion, whereas for deeper quenches, the phase separation is kinetically arrested by the dynamical slowdown of the glassy dense phase. For even deeper quenches a homogeneous attractive glass is expected.<sup>3–5,10</sup> Similar behavior has been reported in a  $\gamma_B$ -crystallin system<sup>6</sup> and in colloidal systems,<sup>7</sup> where a mode coupling theory-like glass line is seen to enter the LLPS

coexistence region. Scenario f was instead described<sup>2</sup> for the gelation of colloidal systems with short-ranged attraction. In this case, the concentrations, for which the dense phase is sufficiently glassy to halt the phase separation, coincide with the high-density equilibrium boundary of the binodal. Upon quenching, the system evolves into large clusters that span the system, and the phase transition is kinetically arrested.<sup>1,2,12</sup> It is still not understood whether this system-dependent behavior is due to different influences of glass formation on the dynamics of the spinodal decomposition or to the fact that the local density cannot be precisely determined experimentally.<sup>11</sup>

In this Letter, we suggest a noninvasive new approach to the study of (arrested) LLPS to experimentally distinguish the two different behaviors. The method exploits an integral, the scattering invariant  $Q$ , to probe the temperature dependence of equilibrium and nonequilibrium states in two-phase systems. We employ Ultra Small Angle X-ray Scattering (USAXS) to collect time-resolved scattering profiles as a function of quench depth. The value of the invariant experimentally extracted from the USAXS profiles at late stages of phase separation is sensitive to perturbations of the shape of the high-density branch of the binodal. The main advantage of the method is

**Received:** July 10, 2020

**Accepted:** August 10, 2020

**Published:** August 10, 2020

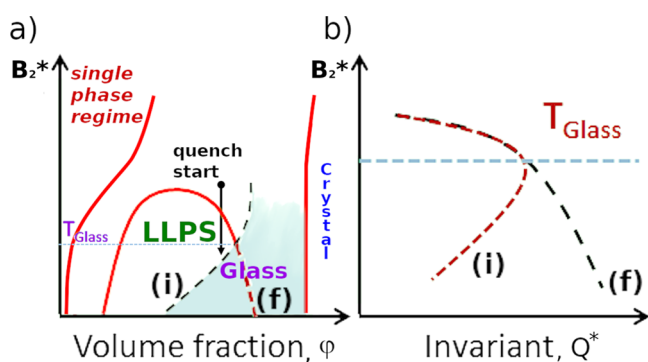


**Figure 1.** (a) General illustration of the liquid–liquid phase behavior of colloidal systems with short-range attraction. The phase diagram is shown using the normalized second virial coefficient,  $B_2^*$ , as a function of the volume fraction.<sup>23</sup> The binodal in this representation is downward-concave for both upper critical solution temperature (UCST) and lower critical solution temperature (LCST) systems. The quenches start above the binodal in the dilute solution (colloidal “gas”)–crystal coexistence region. The two possible scenarios for the interplay between LLPS and glass formation are labeled by i and f, respectively. At  $T_{\text{Glass}}$  the glass transition starts influencing the dynamics of the dense phase, resulting in the slowdown of the growth of the interdomain characteristic length  $\xi$  upon phase separation. (b) Behavior expected for the experimentally extracted invariant,  $Q^*$ , for scenarios i and f.

that it eliminates the need to determine the concentration of the two phases and to manipulate the samples mechanically, while providing insight into the effect of glass formation on the LLPS binodal.

The scattering invariant is a measure of the total scattering power of the sample.<sup>24–26</sup> For isotropic systems, the invariant  $Q$  is related to the scattering intensity  $I(q)$  ( $q$  is the momentum transfer  $q = (4\pi/\lambda)\sin\theta$ ,  $2\theta$  being the scattering angle) by the integral<sup>27</sup>

$$Q = \int_0^\infty q^2 I(q) dq \quad (1)$$

For two-phase systems,<sup>24–26,28,29</sup>  $Q$  is related to the volume fractions of the two phases and to the scattering contrast by

$$Q = 2\pi^2\phi(1 - \phi)\Delta\rho^2 \quad (2)$$

where  $\phi$  is the volume fraction occupied by one of the phases and  $\Delta\rho$  is the scattering contrast between the two phases. In the approximation of internally homogeneous phases,  $Q$  is not influenced by the topology of the two-phase system. Thus, the apparent variation<sup>30</sup> of  $Q$  can be used to probe the boundaries of the two-phase region, regardless of whether the dense phase is in equilibrium or not. Time-resolved evaluation of the invariant allows detection when the two phases have reached a stable composition ( $Q$  reaches a plateau), while studying its dependence on  $T$  captures deviations of the binodal from the expected equilibrium boundary due to the incipient glass formation. The slowdown of the growth of the characteristic length  $\xi$ , representing the real-space correlations between the domains of the two-phase system, during phase separation reflects the increasingly glassy dynamics of the dense phase. The concentration boundaries below the binodal can be evaluated by measuring the invariant at different quench depths and using eq 3 (see below). The contrast  $\Delta\rho$  depends on the concentration difference between the two phases. Inside a binodal, the concentration difference increases for deeper

quenches, while  $\phi(1 - \phi)$  will also increase provided the quench is off-critical and the binodal is not extremely skew (see the Supporting Information, section I). For a liquid–liquid binodal such as the one sketched in Figure 1a, we then expect the value of the invariant to increase with the quench depth. A decreasing invariant is instead due to a reduction of the concentration of the dense phase. This allows for a distinction between the two different scenarios, i and f, in Figure 1 following the phase separation for off-critical quenches. If in the late stage of phase separation the equilibrium boundary is still followed as the kinetics is arresting, scenario f in Figure 1b is observed. If instead the glassy dense phase exists at lower volume fractions than the ideal continuation of the binodal (scenario i), the trend of the value of the invariant will change. Similar approaches employing the scattering invariant have been used to detect phase boundaries,<sup>24,31</sup> to follow the growth of particles,<sup>32</sup> and to detect composition changes in polymer systems.<sup>33</sup>

Ultra Small-Angle X-ray Scattering (USAXS) and Very Small-Angle Neutron Scattering (VSANS) can be applied to study the kinetics of LLPS in protein systems exhibiting both lower and upper critical solution temperature (LCST/UCST) phase behavior.<sup>8,9,34</sup> We followed the phase transition in 4 s intervals up to  $10^3$  s upon an off-critical temperature jump. For shallow quenches, the growth of  $\xi$  follows a power law close to  $\xi \propto t^{1/3}$ , which is consistent with coarsening mechanisms based on diffusion or coalescence.<sup>35–39</sup> For deep quenches, the growth of  $\xi$  in the systems studied initially follows the  $t^{1/3}$  power law (for about the first 30 s) but then slows down and is practically stationary (growth exponent  $\lesssim 0.1$ , up to a resumption of the growth at later stages<sup>9</sup>), indicating an arrested state.

In this Letter, to clarify the interplay between the LLPS boundary and kinetic arrest, we performed a systematic study on two protein systems with short-range attractive interactions: one is BSA–YCl<sub>3</sub> with LCST phase behavior (induced by the specific association of the trivalent salt with the protein) and the other is  $\gamma$ -globulin–PEG1000 with UCST phase behavior (where protein–protein attraction is enabled by the depletion interaction).

Bovine serum albumin (BSA), bovine  $\gamma$ -globulin, polyethylene glycol (PEG1000), and YCl<sub>3</sub> were purchased from Sigma-Aldrich and used as received. Details of sample preparation,<sup>8</sup> characterization,<sup>40</sup> nomenclature,<sup>9</sup> and the USAXS measurements<sup>8</sup> are found in refs 8, 9, and 40. Briefly, high-concentration dense phases were prepared exploiting a first phase separation at room temperature, so to obtain samples lying on the high-density branch of the binodal by removing the dilute phase. A new phase separation was induced by a temperature jump from  $\sim 15$  °C away from the binodal to a final temperature  $T$  within the coexistence region. The resulting quench is therefore always off-critical. Time-resolved USAXS experiments were performed at the ESRF beamline ID02 in Grenoble, France,<sup>34,41</sup> using a sample–detector distance of 30.7 m and an X-ray energy of 12.46 keV to cover a  $q$  range from  $9.0 \times 10^{-4} \text{ nm}^{-1}$  to  $7.5 \times 10^{-2} \text{ nm}^{-1}$ . Samples were filled in 1.0 mm quartz capillaries and inserted horizontally into a Linkam temperature-controlled sample environment with a heating and cooling rate of 80 K/min.

We first consider the BSA–YCl<sub>3</sub> system, which exhibits LCST–LLPS phase behavior.<sup>8,42</sup> The sample is a protein-rich phase obtained from a first phase separation of a parent solution at 175 mg/mL BSA and 40 mM YCl<sub>3</sub>. Figure 2a shows

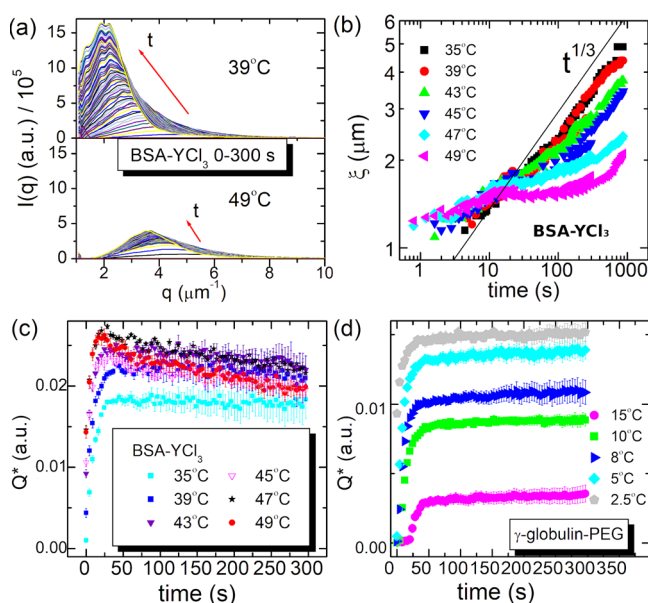


**Figure 2.** (a) Typical ( $t < 300$  s) USAXS profiles for a LCST BSA–YCl<sub>3</sub> sample upon a quench from 10 °C into the two-phase region: for sufficiently deep quenches, the growth of the peak in the scattering profiles arrests. (b) Time dependence of the characteristic length,  $\xi$ , for the same LCST sample upon quenches to different final temperatures, showing the slowdown in the power-law growth. (c) Evolution of the experimental scattering invariant,  $Q^*$ , as a function of time for selected quench temperatures for the LCST BSA–YCl<sub>3</sub> sample. (d) Evolution of  $Q^*$  as a function of time for quenches from 38 °C to selected final quench temperatures for a UCST  $\gamma$ -globulin–PEG sample.

typical USAXS profiles during the initial stage of LLPS for temperature jumps from 10 to 39 °C and 10 to 49 °C. The scattering curve features a peak with position  $q_{\text{max}}$  which increases in intensity and shifts to lower values of  $q$  as coarsening sets in. For low-temperature jumps, the peak moves continuously toward low  $q$ , whereas for high-temperature jumps, after the initial growth, the peak evolution stops, indicating an arrested state. The growth kinetics of the characteristic length  $\xi = 2\pi/q_{\text{max}}$  for selected temperatures is shown in Figure 2b. It is clearly seen that for shallow quenches the growth of the characteristic length  $\xi$  follows a power law close to  $\xi \sim t^{1/3}$ , which is consistent with coarsening mechanisms based on diffusion or coalescence.<sup>35–39</sup> For deep quenches, the growth of  $\xi$  slows down and is eventually almost stationary, indicating a smooth transition from full LLPS to an arrested state.

The experimental scattering invariant  $Q^*$  can be obtained from the USAXS profiles by numerically calculating the limited integral:

$$Q^* = \int_a^b q^2 I(q) dq \quad (3)$$

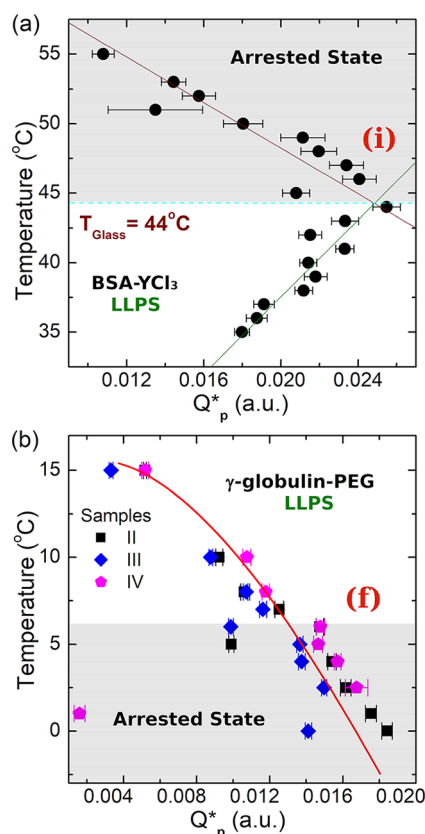
with  $a$  and  $b$  the lowest and highest  $q$  values chosen to define the integration range, including the scattering from the domains of the two phases. The accuracy of the approximation of  $Q$  by  $Q^*$  depends on the  $[a, b]$  range of  $q$  chosen, which is obviously finite (see the Supporting Information, section II).

Figure 2c presents the values obtained for  $Q^*$  as a function of time and for different temperature jumps. The value of the invariant suggests that the final composition compatible with the quench temperature is essentially reached at the initial

stage and maintained throughout the three-stage coarsening.<sup>37</sup> To probe the changes in composition and volume fractions of the dense and dilute phase due to glass formation, we use the values of  $Q^*$  at later stages ( $Q^*$  at plateau,  $Q_p^*$ ). The average in the 100–300 s range is used in the present data treatment. We note that  $Q^*$  increases quickly after phase separation and reaches a constant value for temperatures below 47 °C. Above 47 °C,  $Q^*$  reaches a maximum and then slowly decreases. The reason for this decrease is that at the highest temperatures oscillations in characteristic length and intensity can occur, as the phase separation starts before the final temperature is reached and the characteristic length relaxes to the equilibrium value at the final temperature. Nevertheless, compensating for this effect yields qualitatively similar results (see the Supporting Information, section III).

A similar analysis for the  $\gamma$ -globulin–PEG system exhibiting UCST results in the  $Q^*(t)$  curves shown in Figure 2d. Samples II, III, and IV are again off-critical dense phases produced by a first phase separation of a parent solution of  $\gamma$ -globulin in the range of 110–150 mg/mL with 9 or 10% (w/v) PEG1000.<sup>9</sup> A rather constant plateau in the experimental invariant is reached for all temperatures, featuring at most a very slow increase which may be the manifestation of viscoelastic effects affecting the relative volumes of the two phases.<sup>43</sup> For these samples,  $Q_p^*$  is again calculated as the average in the range of 100–300 s. The nonzero value of the experimental invariant  $Q^*$  at zero time for the deepest quenches is due to an early phase separation peak being immediately present at the beginning of data acquisition.

The results are summarized in Figure 3, showing the temperature dependence of  $Q_p^*$  for both systems. In the case of the BSA–YCl<sub>3</sub> system (Figure 3a),  $Q_p^*$  first increases linearly with increasing temperature. Above 45 °C, it starts to decrease again, down to values lower than the lowest quench temperature probed. This behavior suggests that the dense phase is sufficiently glass-like to determine arrest within the equilibrium coexistence region (Figure 1, scenario i). From linear fits to the increasing and decreasing portion of  $Q_p^*(T)$ , we can estimate  $T_{\text{Glass}} = 44$  °C, at which glass formation below the binodal prevents the dense phase from reaching the equilibrium concentration. The  $\gamma$ -globulin–PEG system shows kinetic arrest at temperatures of about 5 °C and lower, based on the time evolution of  $\xi$ .<sup>9</sup> The  $Q_p^*(T)$  plot (Figure 3b), however, shows an essentially monotonous increase of  $Q_p^*$  as a function of quench depth in the temperature range studied. This behavior is consistent with scenario f, in which the dense phase is likely glassy at concentrations compatible with those of an equilibrium binodal. Thus, we discern between the two scenarios presented in Figure 1 and find that both behaviors are possible and manifest depending on the system. While in the BSA–YCl<sub>3</sub> system the glass transition determines an apparent dense branch of the binodal that bends back toward lower concentrations, the  $\gamma$ -globulin–PEG system features an equilibrium-like binodal even under conditions of kinetic arrest. Importantly, this result is robust with respect to changes in the scattering contrast between the two phases determined by cosolute partitioning. Because it is known that PEG is excluded from the dense phase in LLPS depletion systems<sup>44</sup> and that trivalent cations such as Y<sup>3+</sup> partition preferentially into the dense phase,<sup>45,46</sup> any spurious effect of this kind would result in a behavior opposite of the one observed and can thus be excluded.



**Figure 3.** (a)  $Q_p^*$  (i.e.,  $Q^*$  at plateau) as a function of quench temperature for the LCST BSA–YCl<sub>3</sub> system. The continuous lines are linear fits to the ascending and descending portion of the  $Q_p^*(T)$  data, the crossing identifies a sharp  $T_{\text{Glass}}$  at which glass formation affects the shape of the LLPS boundary. (b)  $Q_p^*(T)$  for three similar UCST  $\gamma$ -globulin–PEG1000 samples (nomenclature as in previous work<sup>9</sup>). The LLPS boundary (red curve, guide to the eye) appears essentially unperturbed in kinetic arrest (shaded area, based on the significant slowdown of  $\xi(t)$ ). The experimental invariant allows discrimination between scenarios i and f in Figure 1. Errors of  $Q_p^*$  are the standard deviations after averaging  $Q^*$  in the plateau range.

Finally, we compare the behavior of  $Q_p^*$  with the LLPS binodal for the BSA–YCl<sub>3</sub> system in Figure 4. The apparent LLPS binodal for an almost identical parent solution<sup>8</sup> shows

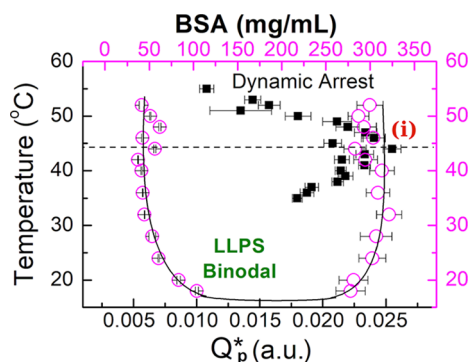


**Figure 4.** Overlay of  $Q_p^*$  as a function of temperature with an experimental LCST binodal for the BSA–YCl<sub>3</sub> system determined from concentration measurements in a previous work.<sup>8</sup>  $Q_p^*$  is very sensitive to deviations from the dense branch of the binodal. The black solid line is a guide to the eye; the dashed horizontal line marks  $T_{\text{Glass}}$ .

LCST phase behavior. The  $Q_p^*(T)$  plot shows clearly a sharp transition due to an increasingly glassy dense phase. Compared to the experimental determination of the concentration, the variation in  $Q_p^*$  is more sensitive to the interplay between LLPS and glass transition.

In conclusion, we exploit time- and temperature-resolved USAXS data to calculate the scattering invariant  $Q_p^*$  at late stages of the phase separation for different quench depths. This procedure yields information on how the relative volumes and concentrations of the dense and dilute phase of two protein-based model LLPS systems change with the quench temperature.  $Q_p^*$  is therefore a sensitive probe of alterations of the binodal due to the glass transition. We find that both reported relations between the LLPS binodal and the glass transition<sup>2,3</sup> can be realized. We speculate that the different behaviors upon dynamic arrest may be related to the nature of the attractive interactions between the proteins (directional charge interaction vs isotropic depletion interaction), simultaneously affecting the dynamics of the glassy phase and the dynamics of phase separation. Further theoretical studies are needed for a better understanding of the mechanism by which the different interactions alter the relation between the two processes and for a more general insight into the relation between the glass transition and phase separation. The different dynamics may stem from the differences between the mostly repulsive glass-like dense phase for the depletion system and the attractive glassy state with YCl<sub>3</sub>, providing stronger directional interactions and longer escape times. Future studies employing existing theories of the glass transition to describe glass formation within the dense protein phase will require more details of the nature of interactions, such as bonding dynamics<sup>47</sup> and specific versus nonspecific interactions.

## ■ ASSOCIATED CONTENT

### Supporting Information

The Supporting Information is available free of charge at <https://pubs.acs.org/doi/10.1021/acs.jpcllett.0c02110>.

Brief discussion of the limits of skewness of the binodal which permits the application of the invariant method, an example of determination of the integration interval for the experimental approximation of the scattering invariant, and alternative treatments to obtain the dependence of the invariant value on the quench temperature (PDF)

## ■ AUTHOR INFORMATION

### Corresponding Author

Fajun Zhang – Institut für Angewandte Physik, Universität Tübingen, 72076 Tübingen, Germany; [orcid.org/0000-0001-7639-8594](https://orcid.org/0000-0001-7639-8594); Email: [fajun.zhang@uni-tuebingen.de](mailto:fajun.zhang@uni-tuebingen.de)

### Authors

Stefano Da Vela – Institut für Angewandte Physik, Universität Tübingen, 72076 Tübingen, Germany; [orcid.org/0000-0002-1700-4759](https://orcid.org/0000-0002-1700-4759)

Nafisa Begam – Institut für Angewandte Physik, Universität Tübingen, 72076 Tübingen, Germany; [orcid.org/0000-0002-5391-8080](https://orcid.org/0000-0002-5391-8080)

Danylo Dyachok – Institut für Angewandte Physik, Universität Tübingen, 72076 Tübingen, Germany

**Richard Santiago Schäufele** – Institut für Angewandte Physik, Universität Tübingen, 72076 Tübingen, Germany

**Olga Matsarskaia** – Institut für Angewandte Physik, Universität Tübingen, 72076 Tübingen, Germany; [orcid.org/0000-0002-7293-7287](https://orcid.org/0000-0002-7293-7287)

**Michal K. Braun** – Institut für Angewandte Physik, Universität Tübingen, 72076 Tübingen, Germany; [orcid.org/0000-0002-9642-7492](https://orcid.org/0000-0002-9642-7492)

**Anita Girelli** – Institut für Angewandte Physik, Universität Tübingen, 72076 Tübingen, Germany

**Anastasia Ragulskaya** – Institut für Angewandte Physik, Universität Tübingen, 72076 Tübingen, Germany

**Alessandro Mariani** – European Synchrotron Radiation Facility, F-38043 Grenoble, France; [orcid.org/0000-0002-3686-2169](https://orcid.org/0000-0002-3686-2169)

**Frank Schreiber** – Institut für Angewandte Physik, Universität Tübingen, 72076 Tübingen, Germany; [orcid.org/0000-0003-3659-6718](https://orcid.org/0000-0003-3659-6718)

Complete contact information is available at:

<https://pubs.acs.org/10.1021/acs.jpcllett.0c02110>

## Notes

The authors declare no competing financial interest.

## ACKNOWLEDGMENTS

The authors thank J. L. Barrat, T. Narayanan, M. Oettel, R. Roth, F. Roosen-Runge, and C. P. Royall for scientific discussions and T. Stehle for sharing lab resources. The authors acknowledge the ESRF for the allocation of beamtime on beamline ID02 and the PSCM for providing their facilities. This work was supported by the DFG. O.M. and A.R. acknowledge Ph.D. fellowships from the Studienstiftung des deutschen Volkes. N.B. acknowledges the Alexander von Humboldt-Stiftung for a postdoctoral research fellowship.

## REFERENCES

- (1) Manley, S.; Wyss, H.; Miyazaki, K.; Conrad, J.; Trappe, V.; Kaufman, L.; Reichman, D.; Weitz, D. Glasslike arrest in spinodal decomposition as a route to colloidal gelation. *Phys. Rev. Lett.* **2005**, *95*, 238302.
- (2) Lu, P. J.; Zaccarelli, E.; Ciulla, F.; Schofield, A. B.; Sciortino, F.; Weitz, D. A. Gelation of particles with short-range attraction. *Nature* **2008**, *453*, 499–503.
- (3) Cardinaux, F.; Gibaud, T.; Stradner, A.; Schurtenberger, P. Interplay between Spinodal Decomposition and Glass Formation in Proteins Exhibiting Short-Range Attractions. *Phys. Rev. Lett.* **2007**, *99*, 118301.
- (4) Gibaud, T.; Schurtenberger, P. A closer look at arrested spinodal decomposition in protein solutions. *J. Phys.: Condens. Matter* **2009**, *21*, 322201.
- (5) Gibaud, T.; Mahmoudi, N.; Oberdisse, J.; Lindner, P.; Pedersen, J. S.; Oliveira, C. L. P.; Stradner, A.; Schurtenberger, P. New routes to food gels and glasses. *Faraday Discuss.* **2012**, *158*, 267.
- (6) Bucciarelli, S.; Casal-Dujat, L.; De Michele, C.; Sciortino, F.; Dhont, J.; Bergenholtz, J.; Farago, B.; Schurtenberger, P.; Stradner, A. Unusual Dynamics of Concentration Fluctuations in Solutions of Weakly Attractive Globular Proteins. *J. Phys. Chem. Lett.* **2015**, *6*, 4470–4474.
- (7) Guo, H.; Ramakrishnan, S.; Harden, J. L.; Leheny, R. L. Gel formation and aging in weakly attractive nanocolloid suspensions at intermediate concentrations. *J. Chem. Phys.* **2011**, *135*, 154903.
- (8) Da Vela, S.; Braun, M. K.; Dörr, A.; Greco, A.; Möller, J.; Fu, Z.; Zhang, F.; Schreiber, F. Kinetics of liquid-liquid phase separation in protein solutions exhibiting LCST phase behavior studied by time-resolved USAXS and VSANS. *Soft Matter* **2016**, *12*, 9334–9341.
- (9) Da Vela, S.; Exner, C.; Schäufele, R. S.; Möller, J.; Fu, Z.; Zhang, F.; Schreiber, F. Arrested and temporarily arrested states in a protein-polymer mixture studied by USAXS and VSANS. *Soft Matter* **2017**, *13*, 8756–8765.
- (10) Olais-Govea, J. M.; López-Flores, L.; Medina-Noyola, M. Non-equilibrium theory of arrested spinodal decomposition. *J. Chem. Phys.* **2015**, *143*, 174505.
- (11) Testard, V.; Berthier, L.; Kob, W. Intermittent dynamics and logarithmic domain growth during the spinodal decomposition of a glass-forming liquid. *J. Chem. Phys.* **2014**, *140*, 164502.
- (12) Testard, V.; Berthier, L.; Kob, W. Influence of the Glass Transition on the Liquid-Gas Spinodal Decomposition. *Phys. Rev. Lett.* **2011**, *106*, 125702.
- (13) Mahmoudi, N.; Stradner, A. Making Food Protein Gels via an Arrested Spinodal Decomposition. *J. Phys. Chem. B* **2015**, *119*, 15522–15529.
- (14) Boire, A.; Renard, D.; Bouchoux, A.; Pezennec, S.; Croguennec, T.; Lechevalier, V.; Le Floch-Fouéré, C.; Bouhallab, S.; Menut, P. Soft-Matter Approaches for Controlling Food Protein Interactions and Assembly. *Annu. Rev. Food Sci. Technol.* **2019**, *10*, 521–539.
- (15) Berry, J.; Brangwynne, C. P.; Haataja, M. Physical principles of intracellular organization via active and passive phase transitions. *Rep. Prog. Phys.* **2018**, *81*, 046601.
- (16) Campbell, A. I.; Anderson, V. J.; van Duijneveldt, J. S.; Bartlett, P. Dynamical Arrest in Attractive Colloids: The Effect of Long-Range Repulsion. *Phys. Rev. Lett.* **2005**, *94*, 208301.
- (17) Kroy, K.; Cates, M. E.; Poon, W. C. K. Cluster Mode-Coupling Approach to Weak Gelation in Attractive Colloids. *Phys. Rev. Lett.* **2004**, *92*, 148302.
- (18) Miller, M.; Frenkel, D. Competition of Percolation and Phase Separation in a Fluid of Adhesive Hard Spheres. *Phys. Rev. Lett.* **2003**, *90*, 135702.
- (19) Segrè, P. N.; Prasad, V.; Schofield, A. B.; Weitz, D. A. Glasslike Kinetic Arrest at the Colloidal-Gelation Transition. *Phys. Rev. Lett.* **2001**, *86*, 6042–6045.
- (20) Eberle, A. P.; Wagner, N. J.; Castañeda-Priego, R. Dynamical arrest transition in nanoparticle dispersions with short-range interactions. *Phys. Rev. Lett.* **2011**, *106*, 105704.
- (21) Valadez-Pérez, N. E.; Liu, Y.; Eberle, A. P. R.; Wagner, N. J.; Castañeda-Priego, R. Dynamical arrest in adhesive hard-sphere dispersions driven by rigidity percolation. *Phys. Rev. E* **2013**, *88*, 060302.
- (22) Foffi, G.; Michele, C. D.; Sciortino, F.; Tartaglia, P. Scaling of Dynamics with the Range of Interaction in Short-Range Attractive Colloids. *Phys. Rev. Lett.* **2005**, *94*, 078301.
- (23) Platten, F.; Valadez-Pérez, N. E.; Castañeda-Priego, R.; Egelhaaf, S. U. Extended law of corresponding states for protein solutions. *J. Chem. Phys.* **2015**, *142*, 174905.
- (24) Feigin, L. A.; Svergun, D. I. *Structure Analysis by Small-Angle X-Ray and Neutron Scattering*; Plenum Press: New York, 1987.
- (25) Lindner, P.; Zemb, T. *Neutrons, X-rays, and Light: Scattering Methods Applied to Soft Condensed Matter*; Elsevier North-Holland, 2002.
- (26) Stribeck, N. *X-ray scattering of soft matter*; Springer, 2007.
- (27) Porod, G. Die Roentgenkleinwinkelstreuung von dichtgepackten kolloiden Systemen. *Colloid Polym. Sci.* **1951**, *124*, 83–114.
- (28) Gerold, V. On the determination of the metastable miscibility gap in ternary alloys from small-angle measurements. I. Theoretical background. *J. Appl. Crystallogr.* **1977**, *10*, 25–27.
- (29) Melnichenko, Y. B. *Small-Angle Scattering from Confined and Interfacial Fluids*; Springer, 2016.
- (30) Glatter, O. *Scattering Methods and their Application in Colloid and Interface Science*; Elsevier, 2018.
- (31) Gerold, V.; Kostorz, G. Small-Angle Scattering Applications to Materials Science. *J. Appl. Crystallogr.* **1978**, *11*, 376–404.
- (32) Liu, J.; Pancera, S.; Boyko, V.; Shukla, A.; Narayanan, T.; Huber, K. Evaluation of the particle growth of amorphous calcium carbonate in water by means of the invariant from SAXS. *Langmuir* **2010**, *26*, 17405–17412.

(33) Niebuur, B.-J.; Claude, K.-L.; Pinzek, S.; Cariker, C.; Raftopoulos, K. N.; Pipich, V.; Appavou, M.-S.; Schulte, A.; Papadakis, C. M. Pressure-Dependence of Poly (N-isopropylacrylamide) Mesoglobule Formation in Aqueous Solution. *ACS Macro Lett.* **2017**, *6*, 1180–1185.

(34) Narayanan, T.; Konovalov, O. Synchrotron Scattering Methods for Nanomaterials and Soft Matter Research. *Materials* **2020**, *13*, 752.

(35) Cahn, J. W. Phase separation by spinodal decomposition in isotropic systems. *J. Chem. Phys.* **1965**, *42*, 93–99.

(36) Dhont, J. K. G. *An Introduction to Dynamics of Colloids*; Elsevier Science B.V., 1996.

(37) Siggia, E. D. Late stages of spinodal decomposition in binary mixtures. *Phys. Rev. A: At., Mol., Opt. Phys.* **1979**, *20*, 595–605.

(38) Bhat, S.; Tuinier, R.; Schurtenberger, P. Spinodal decomposition in a food colloid–biopolymer mixture: evidence for a linear regime. *J. Phys.: Condens. Matter* **2006**, *18*, L339.

(39) Das, S. K.; Roy, S.; Midya, J. Coarsening in fluid phase transitions. *C. R. Phys.* **2015**, *16*, 303–315.

(40) Da Vela, S.; Roosen-Runge, F.; Skoda, M. W. A.; Jacobs, R. M. J.; Seydel, T.; Frielinghaus, H.; Sztucki, M.; Schweins, R.; Zhang, F.; Schreiber, F. Effective Interactions and Colloidal Stability of Bovine  $\gamma$ -Globulin in Solution. *J. Phys. Chem. B* **2017**, *121*, 5759–5769.

(41) Narayanan, T.; Sztucki, M.; Van Vaerenbergh, P.; Léonardon, J.; Gorini, J.; Claustre, L.; Sever, F.; Morse, J.; Boesecke, P. A multipurpose instrument for time-resolved ultra-small-angle and coherent X-ray scattering. *J. Appl. Crystallogr.* **2018**, *51*, 1511–1524.

(42) Matsarskaia, O.; Braun, M. K.; Roosen-Runge, F.; Wolf, M.; Zhang, F.; Roth, R.; Schreiber, F. Cation-induced Hydration Effects Cause Lower Critical Solution Temperature Behavior in Protein Solutions. *J. Phys. Chem. B* **2016**, *120*, 7731–7736.

(43) Tanaka, H. Viscoelastic phase separation in soft matter and foods. *Faraday Discuss.* **2012**, *158*, 371–406.

(44) Lekkerkerker, H. N. W.; Tuinier, R. *Colloids and the Depletion Interaction*; Springer, 2011.

(45) Zhang, F.; Roth, R.; Wolf, M.; Roosen-Runge, F.; Skoda, M. W. A.; Jacobs, R. M. J.; Sztucki, M.; Schreiber, F. Charge-controlled metastable liquid–liquid phase separation in protein solutions as a universal pathway towards crystallization. *Soft Matter* **2012**, *8*, 1313–1316.

(46) Wolf, M.; Roosen-Runge, F.; Zhang, F.; Roth, R.; Skoda, M. W. A.; Jacobs, R. M. J.; Sztucki, M.; Schreiber, F. Effective interactions in protein–salt solutions approaching liquid–liquid phase separation. *J. Mol. Liq.* **2014**, *200* (Part A), 20–27.

(47) Ojovan, M. I. Ordering and structural changes at the glass–liquid transition. *J. Non-Cryst. Solids* **2013**, *382*, 79–86.